UCLA
UCLA Electronic Theses and Dissertations

Title
A Study of the Link between Failure Mechanism of Flip Chip Solder Joints during Electromigration and Their Statistical Life Time Distribution

Permalink
https://escholarship.org/uc/item/22f8625t

Author
Tian, Tian

Publication Date
2012

Peer reviewed|Thesis/dissertation

eScholarship.org Powered by the California Digital Library
University of California

UNIVERSITY OF CALIFORNIA

Los Angeles

A Study of the Link between Failure Mechanism of Flip Chip Solder Joints during Electromigration and Their Statistical Life Time Distribution

A thesis submitted in partial satisfaction

of the requirements for the degree Master of Science

in Statistics

by

Tian Tian

2012

© Copyright by

Tian Tian

2012

ABSTRACT OF THE THESIS

A Study of the Link between Failure Mechanism of Flip Chip Solder Joints during Electromigration and Their Statistical Life Time Distribution

By

Tian Tian

Master of Science in Statistics

University of California, Los Angeles, 2012

Professor Hongquan Xu, Chair

We have employed high resolution synchrotron radiation x-rays 3D imaging techniques, to study the electromigration (EM) failure mechanism in flip-chip solder joints. In these studies, the ex-situ imaging of the early-stage damage evolution at the interface between under bump metallurgy (UBM) layer and solder balls, revealed that the EM induced failure mode of solder joints could be described by Johnson-Mehl-Avrami (JMA) kinetics model. Thus, the JMA kinetics is proposed to serve as a new physical model for life-time prediction of Pb-free solder joints in EM tests. A corresponding Monte Carlo simulation is developed to investigate this simplified failure model and the dependence of the scale parameter and shape parameter in the statistical Weibull equation on the physical factors of the EM tests is studied.

The thesis of Tian Tian is approved.

Yingnian Wu

Juana Sanchez

Hongquan Xu, Committee Chair

University of California, Los Angeles

2012

This thesis is dedicated to my parents.

TABLE OF CONTENTS

LIST OF FIGURES

LIST OF TABLES

ACKNOWLEDGEMENTS

Compiling this report was one of the most gratifying and stimulating experience. I take immense delight in acknowledging all the help I received on the way.

I would like to express my deepest gratitude to my advisor, Prof Hongquan Xu, whose encouragement and support throughout the course of my thesis enabled me to apply statistical methods on my original materials science project. I would also like to extend my sincere thanks to Professor Yingnian Wu and Professor Juana Sanchez from Statistics Department for serving on my thesis committee.

I would like to thank Professor King-Ning Tu in Materials Science and Engineering Department, UCLA for his idea on linking the physical analysis and statistical study on the reliability issues in flip chip technology. I would also like to thank Professor A. M. Gusak in the Department of Theoretical Physics, Cherkasy National University, Cherkasy, Ukraine, for his help on the model building.

I would like to express my sincere appreciation to Dr Daechul Choi, Dr Jung-Kyu Han, and Miss Tanvi Garg for their help on this subject.

Above all, I would like to thank my dear parents for their love and support.

Chapter 1 Introduction

1.1 Packaging technology

Microelectronic industry has two major disciplines: one is chip technologies and the other is packaging technologies. Electronic packaging includes a wide variety of technologies, for protecting enclosed devices from outer damages, mechanically and chemically.[1] Also, electronic packaging techniques provides the electrical interconnections of the I/O on the Si chip and outside electronic system. Electronic packaging is involved with three levels of packaging as illustrated in figure 1.1.[2] The first level refers to the integrated circuit (IC) or chip level packaging. The second level refers to a system level packaging of multi-components with different functions to be assembled onto a board, which is called "motherboard". In some mainframe electronics (i.e. supercomputers), several mother boards carrying a large amount of ICs and several processors are required and connected by connectors and cables so that the extremely highly transactional throughput can be achieved, which is referred to be the third level packaging.

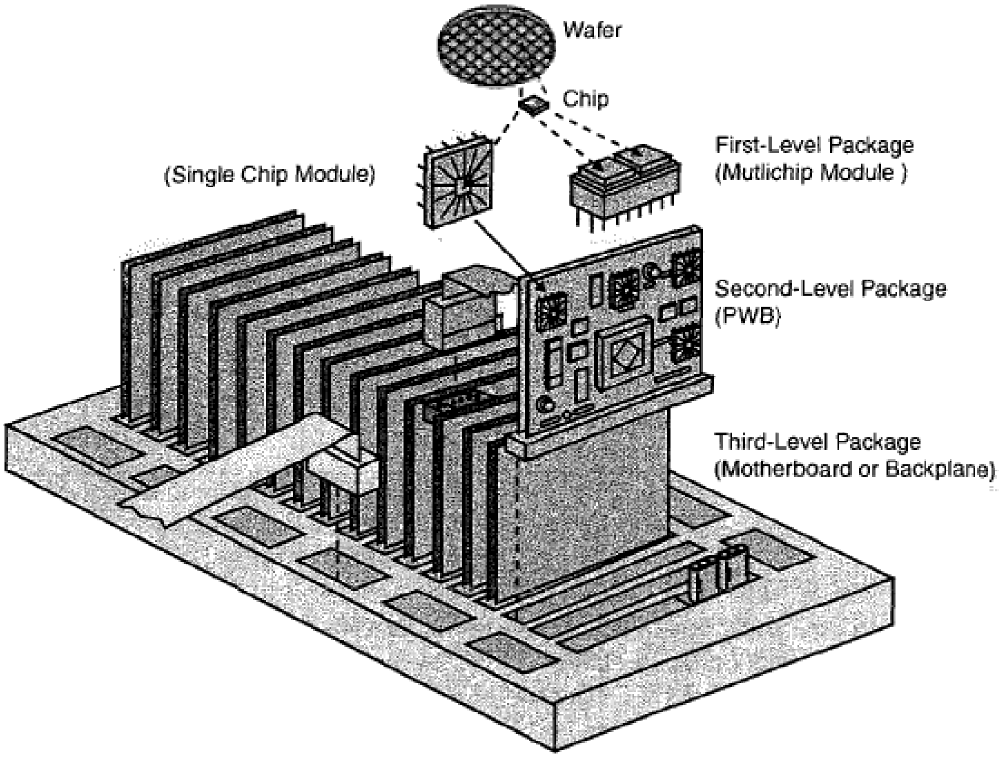

Figure 1.1 Schematic diagram of the hierarchic three packaging level [1]

Flip chip assembly, one of the major technologies of first (chip) level packaging providing the connection of an IC to external circuitry with solder bumps that have been deposited onto the chip pads, was developed to meet the trend of increasing miniaturization of electronic devices and the demand for high density I/O s by IBM in 1960s. The solder bumps are deposited on the chip pads on the top side of the wafer during the final wafer processing step. In order to mount the chip to external circuitry (e.g., a circuit board or another chip or wafer), it is flipped over so that its top side faces down, and aligned so that its pads align with matching pads on the external circuit, and then the solder is flowed to complete the interconnect. The typical processing steps are summarized in figure 1.2. The schematic diagram of the cross-section of a flip chip mount is shown in figure 1.3.[3]

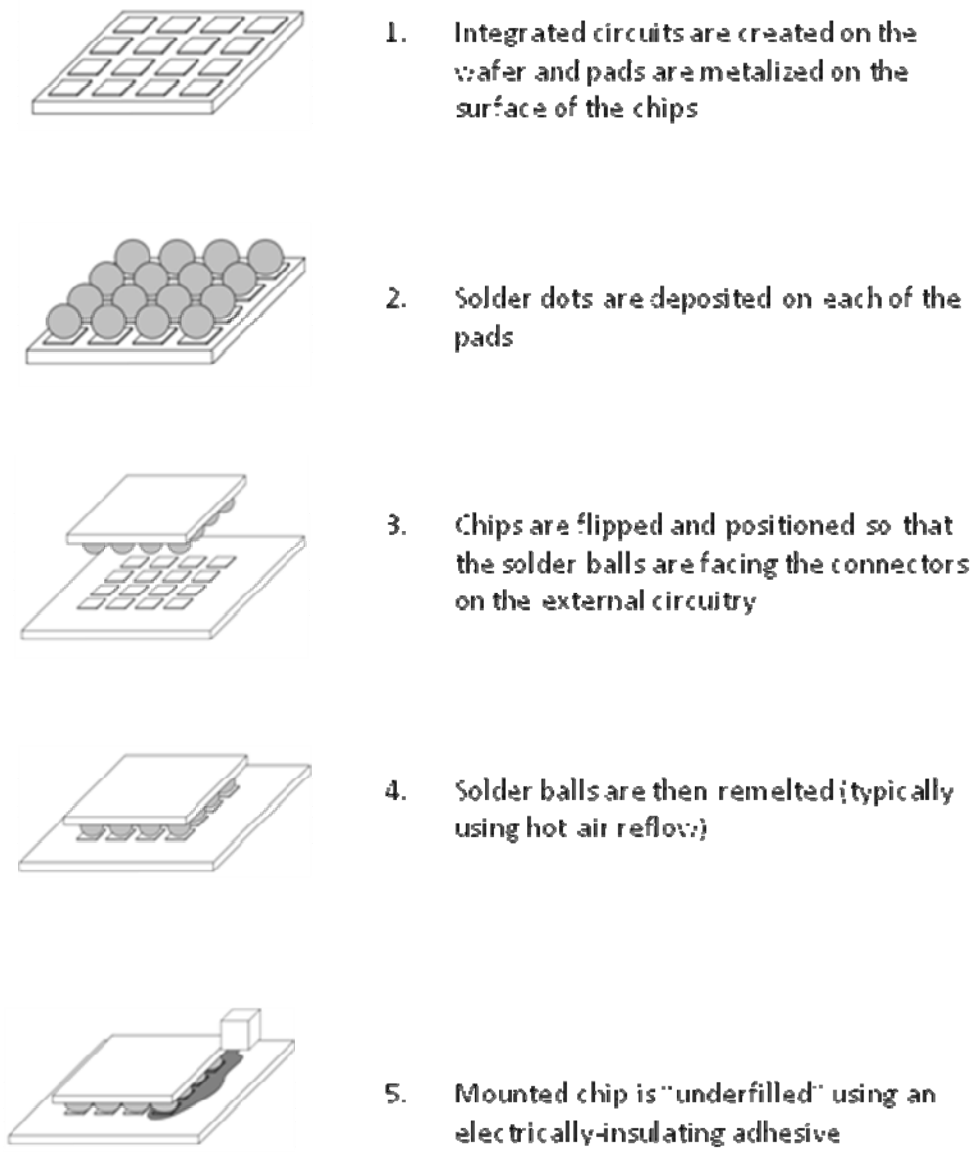

Figure 1.2 Process steps in flip chip assembly [3]

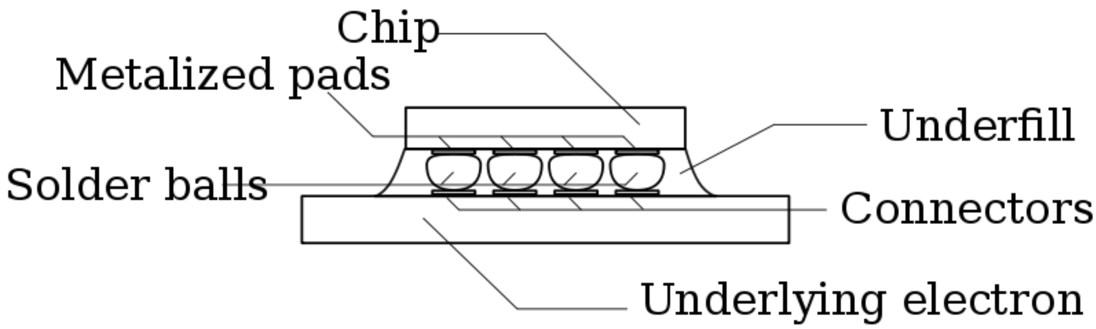

Figure 1.3 Side-view scheme of a typical flip chip mounting [3]

1.2 Electromigration

An ordinary household extension cord conducts electricity without mass transport because the electric current density in the cord is low, about 10^2A/cm^2. The free-electron model of the conductivity of metals assumes that the conduction electrons are free to move in the metal, unconstrained by the perfect lattice of positive ions except for scattering interaction due to phonon vibration. This scattering does not enhance displacement of the ion and it has no net effect on the diffusion of the ion when the electric current density is low. However, the scattering by a high current density, about 10^4A/cm^2 , enhances atomic displacement along with the direction of electron flow. The enhanced atomic displacement and the accumulated effect of mass transport under the influence of electric field (mainly, electric current) are called electromigration (EM). In a thin film interconnect (i.e. solder bumps), the current density is always high enough to facilitate EM, especially at the working temperature of 100^0C. [4]

The diving force of the EM was proposed by Huntington and Grone: [5]

$$F_{EM} = Z^{*}eE = \left(Z_{el}^{*} + Z_{wd}^{*}\right)eE \tag{1.1}$$

where e, E and Z* are the charge of an electron, electric field, and the effective charge number of EM. Z_{el}* is the nominal valence of the diffusing ion and Z_{el}*eE is called the direct force. Z_{wd}* is the effective charge number that represents the effect of momentum exchange between the electrons and the diffusing ion and Z_{wd}*eE is the called the electron wind force. The direct force and the electron wind are in opposite directions. The direction of the direct force is opposite to the electron flow direction, while the electron wind force is in the same direction as that of electron flow and leads to atomic transport from cathode to anode.

The EM induced void formation at the cathode and the hillock formation at the anode of the interconnects, can result in open circuit at the cathode or short circuit at the anode, which is one of the most serious reliability problems. Figure 1.4 shows the typically EM induced damage at the cathode side (chip side) of the solder ball. [6] In this case, the void usually forms at the entrance corner of the electron flow and then propagates along the interface between the metalized pad (which is so called under bump metallization or UBM) and the solder ball until occupying the whole interface.

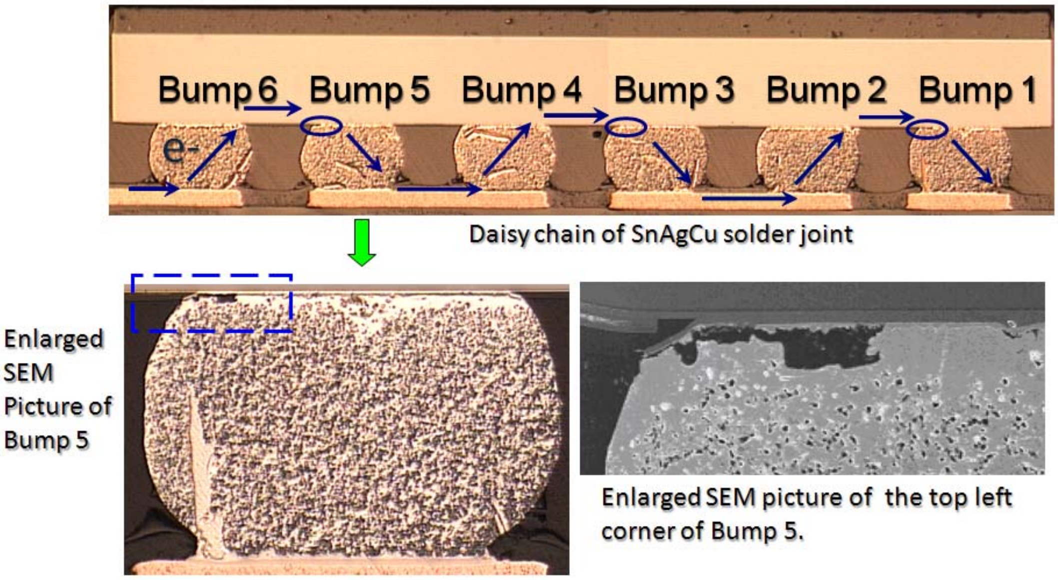

Figure 1.4 EM induced failure in flip-chip solder joints [6]

1.3 Black's equation of mean-time-to-failure (MTTF)

Since EM is a critical reliability issue in packaging technology, people are certainly interested in the estimation of the EM induced time-to-failure (TTF) of the certain electronic product. In 1967, James R. Black contributed to the concept of Mean-Time-To-Failure (MTTF) by relating it to current density and temperature,[7-9]

$$\mathrm{MTTF} = Aj^{-n} \exp\left(\frac{E_a}{kT}\right), \quad A = \left[\left(\rho\frac{\lambda}{\nu}\right)\sigma_{cross}\right]^{-1} \qquad (1.2)$$

where j is current density of electron flow, E_a is the activation energy in electron volts, k is the Boltzman constant and T is the temperature of the film, ρ is the resistivity per unit volume, λ is the mean free path of electron with an average velocity ν, σ_{cross} represents the effective cross section of the target (cm^2). The pre-factor A here only depends on the inherent properties of the material. MTTF thus depends on the current density and temperature. As the current density or temperature increases, the MTTF decreases. The value of curernt density exponent n whether it is 1, 2 or a larger number is still controversial. However, in most of the studies of MTTF the current density exponent n has been reported to be 2.[8] The model is abstract, not based on a specific physical model, but flexibly describes the failure rate dependence on the temperature, the electrical stress, and the specific technology and materials. More adequately described as descriptive than prescriptive, the values for A, n, and E_a are found by fitting the model to experimental data. Black's equation is valuable since in a short period of time it helps to estimate the actually life time under normal device operating conditions by testing the device at accelerated condition of high temperature and high current stress levels.[10]

1.4 JMA Theory of Phase Transformation

The JMA theory was presented by John, Mehl (1939) and Avrami (1941), which is a classical analysis of phase transformation described by the kinetic process of nucleation and growth. [11-13]

In the JMA theory, we can consider V to be the total volume involved in the transformation, in which V_T and V_U is the transformed volume and untransformed volume, respectively, as shown in Figure 1. 5.

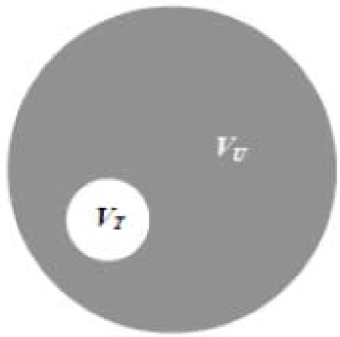

Figure 1.5 A diagram representing the untransformed (V_U) and transformed (V_T) volume

$$V = V_U + V_T \tag{1.3}$$

or

$$1 = X_U + X_T \tag{1.4}$$

where $X_U=V_U/V$ and $X_T=V_T/V$ are the fraction of untransformed volume and transformed volume, respectively. It is assumed that (i) transformation occurs by nucleation and growth, (ii) nucleation is random in space and time and (iii) each of the transformed region has the same isotropic growth rate of R_G, then the number of newly transformed regions in the untransformed volume in the time interval between t and t+dτ is given by:

$$N = R_N V_U d\tau \tag{1.5}$$

where N is the number of newly transformed regions which nucleates in the untransformed volume, R_N is the rate of nucleation (the number of nuclei per unit time per unit volume), t is the initial time and dτ is the time interval.

Since isotropic growth rate has been assumed for each transformed region, the radius r of the spherical volume of the transformed region that originates at τ as shown in figure 1.5 is given by:

$$r = R_G(t-\tau) \tag{1.6}$$

and therefore the volume of the transformed region (V_T) is:

$$\begin{aligned} V_\tau &= \frac{4\pi}{3} R_G^3 \left(t-\tau\right)^3 && for\ t > \tau \\ V_\tau &= 0 && for\, t \le \tau \end{aligned} \tag{1.7}$$

The differential change of the untransformed volume can thus be written as:

$$-dV_U = NV_\tau = V_\tau R_N V_U d\tau \tag{1.8}$$

The negative sign here represents decrease of the untransformed volume. Also on differentiating Eq (1.3), we get,

$$-dV_U = dV_T \tag{1.9}$$

and,

$$dV_T = NV_\tau = V_\tau R_N V_U d\tau \tag{1.10}$$

by integrating Eq (1.10) and substituting Eq (1.7), we have,

$$V_T = \frac{4}{3}\pi \int_{\tau=0}^{\tau=t} V_U R_N R_G^3 \left(t-\tau\right)^3 d\tau \tag{1.11}$$

In the initial stage of transformation, we can conveniently assume that the volume of untransformed region is much more than the volume of the transformed region, $V_U \gg V_T$, and thus the entire volume, V, can be approximated to untransformed volume V_U. Also by assuming that the nucleation rate is constant with time, we can re-write the Eq (1.11) to be:

$$X_T = \frac{V_T}{V} = \frac{1}{3}\pi R_N R_G^3 t^3 \qquad (1.12)$$

The Eq (1.12) is only valid for initial stages of transformation where the transformed regions do not interfere with each other (i.e. no impingement or no overlapping occurs). While at the later stages of transformation, both impingement and overlapping take place as shown with the example of raindrops falling on the surface of a pond. To include the effect of interference, a concept of "extended volume" V_{ext} has been introduced between the time interval t and t+dτ as:

$$dV_{ext} = V_\tau R_N \left(V_U + V_T\right) d\tau \qquad (1.13)$$

where dV_{ext} represents the differential change in volume of both transformed and untransformed regions. The growth of nuclei in the transformed region does not affect the untransformed region, which are called “phantom nuclei”. The growth of phantom nucleation does not contribute to the new phase transformation.

By arranging Eq(1.3)

$$1 = \frac{V_U}{V} + \frac{V_T}{V}$$
$$\left(1 - \frac{V_T}{V}\right)V = \left(\frac{V_U}{V}\right)V,$$

we can get $$\left(1-\frac{V_T}{V}\right)\left(V_U+V_V\right)=V_U \tag{1.14}$$

By substituting Eq (1.14) into Eq (1.10), we have

$$dV_T=\left(1-\frac{V_T}{V}\right)V_\tau R_N\left(V_U+V_T\right)d\tau=\left(1-\frac{V_T}{V}\right)dV_{ext} \tag{1.15}$$

By rearranging Eq (1.15), we have

$$dV_{ext}=\frac{-Vd\left(1-\frac{V_T}{V}\right)}{\left(1-\frac{V_T}{V}\right)}\text{ , then } V_{ext}=-V\ln\left(1-\frac{V_T}{V}\right)+cons. \tag{1.16}$$

The Eq (1.16) can be also written as

$$X_T=1-\exp\left(-X_{ext}\right), \tag{1.17}$$

where $X_T=\frac{V_T}{V}$, $X_{ext}=\frac{V_{ext}}{V}$, and $X_{ext}=\frac{4}{3}\pi\int_{\tau=0}^{\tau=t}R_N R_G^3\left(t-\tau\right)^3 d\tau$. If the nucleation rate is random and continuous, and the growth rate is isotropic and linear with time, in three-dimension case, $X_{ext}=\frac{1}{3}\pi R_N R_G^3 t^4$. Therefore, $X_T=1-\exp\left(-Kt^4\right)$, where $K=\frac{1}{3}\pi R_N R_G^3$.

We assumed a dependence of t^4 for nucleation and growth in the above analysis. However, in general, time dependence should depend not only on the dimension of transformation, but also on the mode of nucleation and growth. Thus, the universal form of the JMA equation can be written as

$$X_T = 1 - \exp\left(-Kt^n\right) = 1 - \exp\left[-\left(\frac{t}{\tau_0}\right)^n\right], \text{ where } K = \left(\tau_0\right)^{-n}, \tag{1.18}$$

n is the mode parameter of transformation.

1.5 Weibull distribution in statistical analysis of time to failure

In 1951 Waloddi Weibull presented the Weibull distribution in his groundbreaking paper, “A statistical distribution function of wide applicability” in the Journal of Applied Mechanics, which is the hallmark paper of Weibull analysis. The first example in the paper concerned the yield strength of Bofors steel. [14] Today, this distribution is widely used in dealing with the time to failure of electronic devices. It can be derived theoretically as a form of extreme value distribution, governing the time to occurrence of the "weakest point" of many competing failure processes. For example, if a system consists of N identical components in series, and the system fails when the first of these components fails, then system failure times are the minimum of N random component failure times. The extreme value theory says that, independent of the choice of component model, the system model will approach a Weibull distribution as N becomes large.

The Weibull probability density function (PDF) is

$$f(t) = \left(\frac{\beta}{\eta}\right)\left(\frac{t}{\eta}\right)^{\beta-1} \exp\left[-\left(\frac{t}{\eta}\right)^{\beta}\right], \tag{1.19}$$

where η is the characteristic time when 63% of the components fail., t is the time to failure and β is the shape parameter, which is the slope of the Weibull distribution plot. The cumulative distribution function (CDF) is

$$F(t) = 1 - \exp\left[-\left(\frac{t}{\eta}\right)^{\beta}\right], \tag{1.20}$$

where F(t) is the percentage of failures at time t. The failure rate is defined the number of new failures occur within a small time interval, $\lambda(t) = \dfrac{f(t)}{1-F(t)} = \left(\dfrac{\beta}{\eta}\right)\left(\dfrac{t}{\eta}\right)^{\beta-1}$. The failure rate is constant when the shape parameter β =1, decreases for β <1, and increases when β >1. This implies that there is very little difference in the time to failure among all components when β >1, which means that there is a very short time period between first failure and the last failure. In most of real cases, β >1 is more desirable in the microelectronic industry for reasons of reproducibility. [15]

1.6 Summary and Discussion

Eq (1.18) and Eq(1.20) show that the JMA equation and Weibull distribution are in a same mathematical form. We believe that there is an intrinsic link between these two equations, though they are applied in different fields.

Chapter 2. Experiments and Model

2.1 Introduction

The void formation induced by EM at the cathode side is one of the most serious reliability concerns in the electronic packaging industry [4]. One key study in this field is how to predict the life time of the solder joints in the accelerated life tests within an acceptable testing time. Thus a reasonable modeling work basing on the real failure mechanism during accelerated EM tests, is valuable to be applied to predict the life time of the test vehicles under a certain stressing condition.

In the past few years, pancake-shape void formation and propagation was found to be the main failure mode of flip chip solder joints in the EM tests, since the unique line-to-bump geometry results in significant current crowding effect at the current entrance of the solder bumps. Accordingly, a few kinetics models describing the pancake-type void propagation has been built-up [16-18].

However, the main experimental evidence of the previous modeling works is SEM observation. Restricting the study of the flip chip joint to the traditional two-dimensional (2D) examination procedure can yield two problems. One is the difficulty in uncovering the kinetics in the real rest vehicle during EM, especially at the early stage, which requires nondestructively monitoring. The other one is that a 2D measurement will bring more uncertainties of the void growth measurement in a real three-dimensional (3D) structure. The both problems would result in the main limitation of the pancake-type void modeling works.

Recently, the applications of synchrotron based x-rays non-destructive 3D imaging techniques enabled us avoid the 2D problems just outlined. A few experiments have been done by our group. The quantitative ex-situ computed tomography study was conducted at beamline 8.3.2 at the Advanced Light Source (ALS) of Lawrence Berkeley National Laboratory (LBNL), to measure the effective charge number Z* of eutectic SnPb during EM tests precisely, by monitoring the dramatic growth of pre-existed voids inside the solder.[19] Moreover, the synchrotron-radiation computed laminography (SRCL), an alternatively 3D imaging technique, which is designed for flat samples, was employed to study the EM-induced voids formation and evolution at the interface between 7.5µm thick Cu UBM and SN100C(Sn, Cu (0.65%), Ni (500ppm), Ge (60ppm), Bi (110ppm), Pb (140 ppm)) solder bump[20], at the high energy beamline ID15A at the European Synchrotron Radiation Facility (ESRF). The imaging results showed that the mode of damage evolution at the interface was quite different from the failure mode of pancake-shape void formation and propagation model at the early stage. And the results were proposed to be fitted by Johnson-Mehl-Avrami(JMA) phase transformation theory. And an intrinsic link between JMA model and the Weibull distribution of life time was discussed.

Basing on the synchrotron radiation based x-rays 3D imaging observations, we propose that the JMA phase transformation model can serve as a new physical model for life time prediction of Pb-free solder joints in EM tests. In this thesis, Monte Carlo simulation is employed to build up a simplified mathematical model of JMA induced failure. By investigating this model, we would like to investigate the dispersion of time-to-failures (TTFs) dependence on two physical parameters (nucleation frequency and growth velocity) and one geometrical parameter (failure criteria).

2.2 Experiments

2.2.1 Sample description

The figure 2.1(a) shows the test vehicle we used in this study provide by National Semiconductor Cooperation, a single printed circuit board (PCB) with 4 identical WL-CSP test chips labeled as U1, U2, U3, U4. The dimension of one chip is 3000μm×3000μm and consists of 36 solder balls. The diameter of each solder ball is 250 μm. The composition of the solder ball used here is SN100C. The flip chip configuration and dimension are shown by the figure 2.2(a), a schematic diagram of the cross-section of the sample tested.

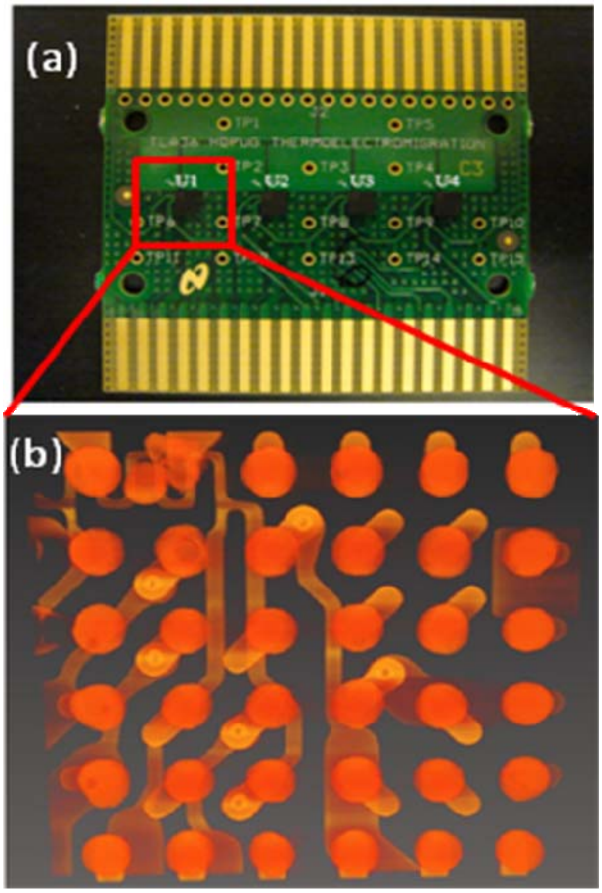

Figure 2.1 (a) a single test PCB with 4 test chips labeled as U1, U2, U3 and U4, (b) reconstructed micro-tomography 3D image of a failed test chips, with a melted solder ball at the upper left corner region.

2.2.2 EM test system in UCLA

To collect the life times of the test vehicles for statistical analysis, we conducted a series of the accelerated EM tests in UCLA. During the EM tests, the four test chips on a board were connected in series and current flowed through only one pair of bumps in each chip. When one of the four chips failed, a hook wire was soldered to bypass the failed chip and maintained the current flowed through the remaining chips. For example, if U2 failed (figure 2.1(a)), the TTF of U2 would be recorded, the failed unit would be bypassed and the subsequent EM test was pursued till all of the four chips are failed.

The EM tests were running with two different current densities: 7.5×10^3A/cm^2 (low-current), and 1×10^4A/cm^2 (high-current), at the same temperature 125°C. For each test condition, four test boards were tested (i.e. 16 test chips in series), thus there were 16 TTFs.

2.2.3 Synchrotron radiation x-rays 3D imaging

One failed chip was imaged, shown in figure 2.1(b) by micro-tomography technique at beamline 8.3.2 at the ALS, LBNL. The principle of this technique has been described in detail elsewhere [21]. In this technique, the parallel x-rays with a beam size of 35mm (width) by 4.6 mm (height) passed through the sample that was mounted the rotation stage. The transmitted x-rays impinged on a 0.5 mm thick $CdWO_4$ single crystal scintillator that fluoresced the image as visible light that replayed via magnification lenses on the Cooke PCO 4000 CCD imaging camera (4008×2672 pixels). The contrast of the images comes from different attenuation lengths of metals caused by x-rays absorption. During data collection, the sample was rotated by 180^0C, in angular increments of 0.125^0, and an image recorder at each angular step with 1000ms exposure time. Reconstruction of the 3D images was conducted with Octopus software package from the University of Ghent. Viewing and analysis of the images were performed using the commercial 3-D visualization software Avizo 6.0. The voxel size used was 1.8μm, as set by the lens magnification and CCD pixel size. Figure 2.1(b) is the 3D tomography reconstructed image of one failed chip, showing that there are 36 bumps in the chip and the second bump on the upper left corner has failed by EM.

To study the early damage evolution at the interface between UBM and solder ball, the ex-situ SRCL imaging experiments were conducted on the high energy beamline ID15A at the ESRF [20]. The general technique has been described elsewhere [22, 23]. The main difference between laminography and tomography is that in the former one the rotation axis of the sample is not perpendicular to the x-ray beam and the algorithm is developed for imaging regions of interest (ROI) in flat, especially. Before the start of the accelerated EM tests, the solder joints were scanned for initial imaging in 3D as reference. After a given hours of EM stressing, the samples were re-scanned to check the changes inside. In the ex-situ SRCL imaging, two same chips were powered with the same two current densities: $7.5\times10^{3}A/cm^{2}$ (low-current), and $1\times10^{4}A/cm^{2}$ (high-current), and both were at the same temperature $125^{o}C$, which is same as the one we used in the statistical study. Figure 2.2(b)-(d) show the digital slice images of the interface between the solder ball and UBM from top view at different time stages, which was stressed by low-current density. Similarly, figure 2.2(e)-(g) show the voids evolution at the top interface of the sample stressed by high-current density. The voxel size of the slice images is about 0.84μm.

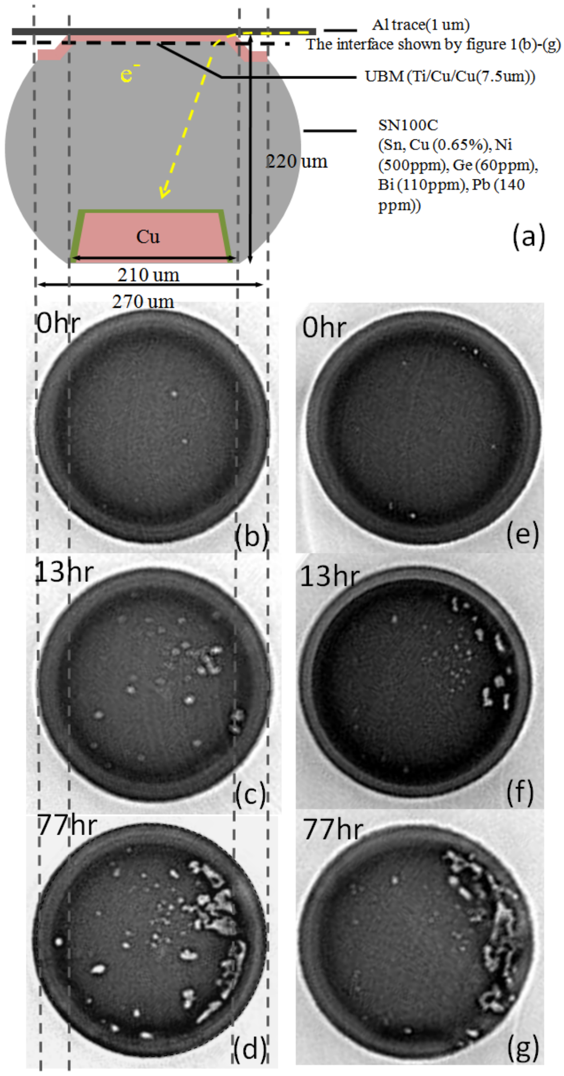

Figure 2.2(a) The schematic diagram of the cross-section of a tested solder joint, showing the configuration and dimensions of the sample. Figure 2.2(b)-(d) show the SRCL digital slice images of the sample I at the interface between the solder ball and the UBM before EM test (figure 2.2(b)), after 13 hr EM test(figure 2.2(c)), after 77 hr EM test(figure 2.2(d)), respectively, by 7.5×10^3 A/cm^2, at 125°C. Figure 2.2(e)-(g) show the SRCL digital slice images of the sample II at the interface between the solder ball and the UBM before EM test (figure 2.2(e)), after 13 hr EM test(figure 2.2(f)), after 77 hr EM test(figure 2.2(g)), respectively, by 1×10^4 A/cm^2, at 125°C.[20]

2.3 Experimental Results

2.3.1 Statistical analysis by Weibull Distribution

Statistical study of 16 TTFs with each EM condition has been carried, show in table 2.1 The cumulative distribution function (CDF) of the TTFs can be fitted by Weibull distribution [20]

$$F(t) = 1 - \exp\left(-(t/\eta)^{\beta}\right), \tag{1.20}$$

shown in figure 2.3(b), to get

1) η=619.3hr, β=2.34 under the high-current EM condition;

2) η=3469hr, β=1.85 under the low-current EM condition,

where η is the characteristic life time of the reliability under a certain testing condition, β is the shape parameter.

EM condition	TTFs
1×10^4A/cm^2 at 125^0C	571.5, 566.5, 483.5, 735.5, 475.5, 334.5, 418.5, 1205.1, 661.5, 370.0, 342.5, 370.5, 661.5, 475.5, 159.0, 932.5,
7.5×10^3A/cm^2 at 125^0C	2873.5, 972.0, 3319.0, 2291.0, 2085.0, 1920.0, 3172.5, 1791.0, 696.0, 1921.0, 3234.0, 1945.0, 3890.0, 5818.0, 6420.0, 6700.0

Table 2.1 16 TTFs in each EM testing condition

2.3.2 Physical analysis by JMA phase transformation model [20]

The SRCL imaging results, shown by figure 2.2(b-g), reveal that in real cases, the nucleation sites of voids are scattered on the interface at the early stage, even though later the growth rate of the voids in the current crowding region would be faster. This process is similar to the phenomenon of phase transformation described by JMA kinetics model [20],

$$X_T = 1 - \exp\left(-\left(t/\tau\right)^n\right), \tag{1.18}$$

where X_T is the degree of phase transformation at the time t, τ is the characteristic time of the transformation, and n is the parameter indicating the mode of new phase growth. Here we can define the degree of the void occupying at the interface $A_v/A_i=X_T$ and τ is the characteristic time of the voids growth. By measuring the voids area A_v at different time stage and whole interface area A_i, and thus fitting the relationship between $\ln\left(-\ln\left(1-X_T\right)\right) \sim \ln t$ linearly, we can get the value of both τ and n under each testing condition, shown in figure 2.3(a),

1) τ=768.5hr, n=0.7 under the high-current EM condition;

2) τ=3905.7hr, n=0.52 under the low-current EM condition.

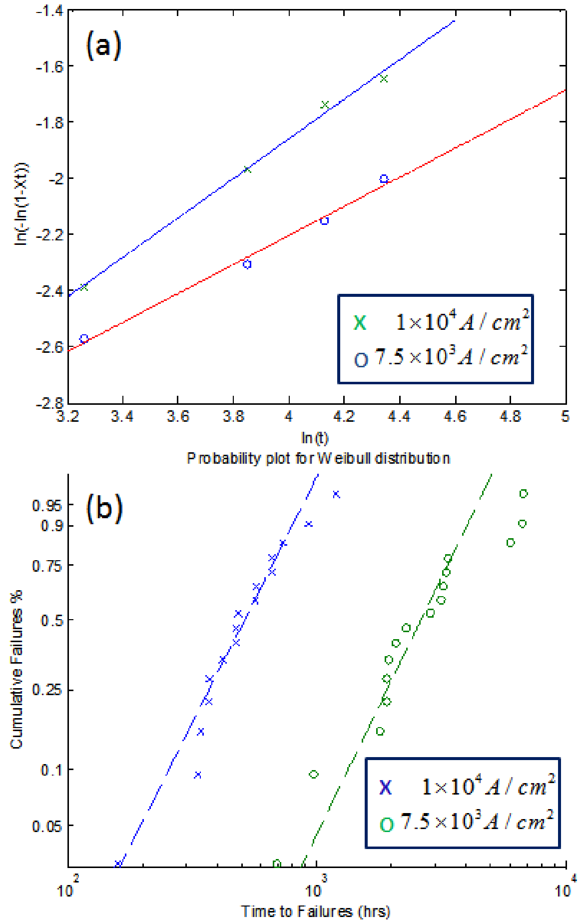

Figure 2.3(a) illustrats the linear relationship between $\ln\left(-\ln\left(1-X_T\right)\right) \sim \ln t$ of sample I (stressed by 7.5×10^3 A/cm^2 at 125^{o}C) and sample II (stressed by 1×10^4 A/cm^2 at 125^{o}C), respectively, fitted by JMA-like model. The slope of the linear line is n (mode of void growth), while the intercept of the line is $-n\ln\tau$. The parameters of n and τ of the both samples by fitting the JMA-like model, were shown in Table 2.2. Figure 2.3(b) shows the distribution of the TTFs, measured from two groups of solder joints tested at 125^{o}C, by 7.5×10^3 A/cm^2 and 7.5×10^3 A/cm^2 respectively. The shape parameters and characteristic life time of them fitted by Weibull distribution, are shown in Table 2.2.

EM condition	Mode of void growth n	Characteristic time τ (hr)	Shape parameter β	Characteristic time η (hr)
7.5×10^{3}A/cm^{2} at 125^{0}C	0.52	3905.7	1.85	3469
1×10^{4}A/cm^{2} at 125^{0}C	0.70	768.5	2.34	619.3

Table 2.2 A summary of the parameters of n, τ, β, η fitted by JMA-like model and Weibull distribution under two EM test conditions.

2.3.3 Intrinsic link between Weibull distribution and JMA theory

From the above analysis, clearly, we found that Eq (1.18) and (1.20) are in a same format and moreover the values of η and τ are in a good agreement, when they are under the same EM test condition. Thus, the nondestructive 3D imaging of the early stage void evolution at the interface between UBM and solder ball was proposed to be a rapid life prediction method, by applying the JMA kinetics model [20]. In our previous work, a simple explanation was provided to support the intrinsic link between JMA theory and Weibull distribution, even though they are used in two distinguished region: the link between these two models comes from the similarity as the weakest-link distribution in them.

2.4 Monte Carlo study on the model of "JMA induced mathematical failure"

The proposed application of JMA model in EM life time prediction bases on the observation of that the EM-induced failure of solder contact may happen not by gradual propagation of one pancake void but instead by stochastic nucleation and lateral growth of many voids, when thinker UBMs are used. To understand this proposed model deeper, we start trying to investigate a very simplified mathematical model—"JMA induced mathematical failure". The model is built up with the following assumptions:

1) There are M solder contacts in the scheme and only one failure mode of these contacts: JMA nucleation and lateral growth of voids until full transformation of a contact into void.

2) Each nucleated circular island grows with constant velocity V, which is typical for JMA model.

3) The nucleation frequency per unit area ν is the same everywhere and constant in time.

4) The contact is a square area of L×L, where L is a side length.

5) The time of full coverage of void phase in a contact is treated as time-to-failure (TTF) in the simulation.

With the three mentioned physical parameters, V(m/s), $\upsilon(1/m^2s)$, L(m), we can introduce a non-dimensional parameter $G=V/\upsilon L^3$. We suppose, this parameter, and only it, determines the statistics of TTFs. Due to existence of non-dimensional combination of three parameters, we can construct the characteristic time, characteristic length, and characteristic velocity in several ways. For example:

$$t_0 = \frac{1}{\nu L^2},\ l_0 = L,\ V_0 = \nu L^3 \ . \tag{2.1}$$

Here $t_0 = \frac{1}{\nu L^2}$ is an average time between successive nucleations in a whole contact area. Then non-dimensional time, length and velocity are

$$tt = \frac{t}{t_0} = \nu L^2 t,\ \ ll = \frac{l}{l_0},\ VV = \frac{V}{V_0} = \frac{V}{\nu L^3} \equiv G\,. \tag{2.2}$$

Another possible choice is:

$$t_1 = \left(\frac{1}{\nu V^2}\right)^{1/3},\ l_1 = Vt_1 = \left(\frac{V}{\nu}\right)^{1/3},\ V_1 = V \ . \tag{2.3}$$

Here $t_1 = \left(\frac{1}{\nu V^2}\right)^{1/3}$ is an approximate time of covering an essential part of area. We can predict that the MTTF (mean time to failure) should be proportional to this characteristic time:

$$MTTF = zt_1 = z\left(\frac{1}{\nu V^2}\right)^{1/3}. \tag{2.4}$$

Yet, we shall use the first choice (Eqs.(2.1) and(2.2)) of characteristic parameters since in numerical simulation it is more convenient to use the same non-dimensional size of the sample (in our case = square 1×1) and to change the non-dimensional velocity. So far we did not manage to solve this problem analytically, but the above introduced scaling allows us to obtain rather general results by the computed modeling of the non-dimensional problem.

The main points of the algorithm are as follow:

1) We treat the square sample ll×ll=1×1.

2) We divide both horizontal and vertical axes into N intervals, where $d_{xx}=d_{yy}=1/N$.

3) Each cell of area $d_{xx}\times d_{yy}=1/N^2$ can be in two states – “old” and “new”.

4) At each time step d_{tt}, all the elements of “old” state have a probability dp to transform to be that of “new” state, where

$$dp = \nu dxdydt \equiv \frac{dx}{L}\frac{dy}{L}d\left(\nu L^2 t\right) = dxx \cdot dyy \cdot dtt = \frac{dtt}{N^2}$$

Once an element (i,j) gets transformed, the time will be recorded as tt(i,j)

5) The successful nucleation site (i,j), at some time tt(i,j), becomes the center of transformation circle propagating with velocity VV=G, so that at any later time tt>tt(i,j) any cell in the circle of radius VV×(tt-tt(i,j)) with the center in cell (i,j) is obligatory “new”.

6) The time moment TTF(G), at which the last cell becomes new, is being written to memory as TTF(k;G), where k is a number of runs. After running the same program with the same non-dimensional velocity M times (1<k<M), we obtain an array of TTF, which could be statistically processed by standard code giving probability distribution (PDF), cumulative probability distribution (CDF) at given VV=G.

7) We change G in reasonable measures (0.1<G<5) and find the dependencies of Weibull CDF non-dimensional parameters η,β on G. A similar investigation can be done on $\frac{dtt}{N^2}$.

$$F(tt) = 1 - \exp\left(-\left(\frac{tt}{\eta} \right)^{\beta} \right).$$

.

Chapter 3 Results of Simulation and Discussion

The simulations were run in MATLAB. A sample code is attached in the chapter 5. In this example, we define the number of the units in the area is $N^2=100^2$, the nucleation rate is p=0.0001, the growth rate is VV=0.1. Figure 3.1 (a-d) shows a typical phase transformation progress generated by the sample code, where the white color represents the new phase and the black color represents the old phase. In the figure 3.1, the phase transformation situations at four different time stages are shown (a) at t=30, when X_T=10%, (b) at t=47, when X_T=30%, (c) at t=66, when X_T=60%, and (d) at t=94, when X_T=90%.

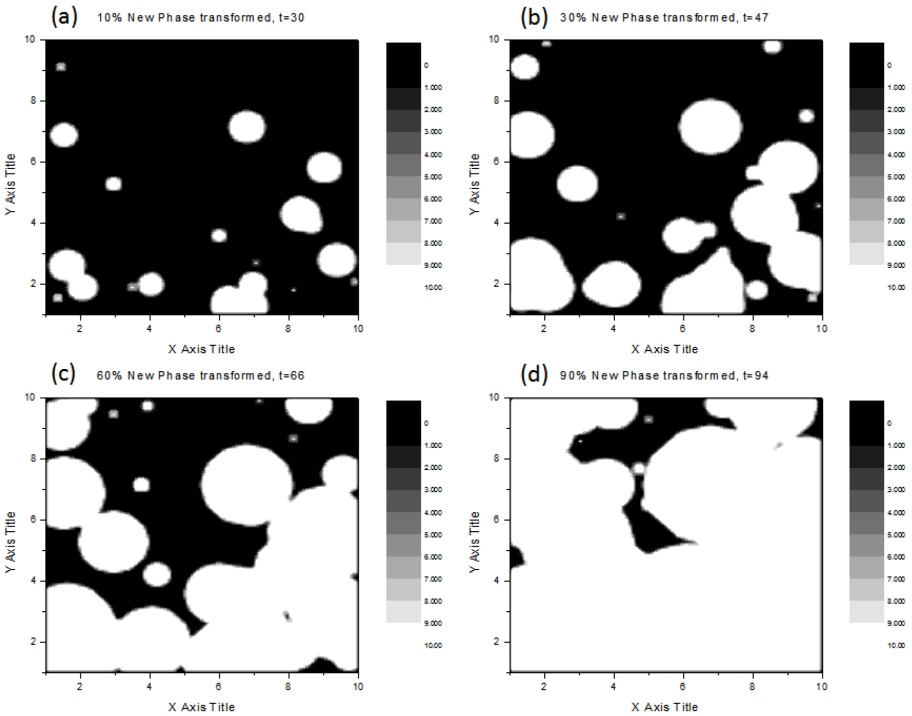

Figure 3.1 A typical example of the phase transformation process in the simulation by the sample code in chapter 5: (a) "new" (white) phase coverage percentage X_T=10%, the non-dimensional time t=30; (b) X_T=30%, t=47 ; (c) X_T=60%, t=66; (d) X_T=90%, t=94.

If we run this sample code 100 times, then we will have 100 time-to-failures (TTFs), which is the time needed for new phase to occupy a whole square, shown in table (3.1). The Weibull fit of its CDF is shown in figure 3.2 by MATLAB. And we get the characteristic time of the Weibull fit η=128.197, shape parameter β=7.066.

107	123	108	112	113	106	169	100	115	119
116	111	134	121	112	110	118	132	105	129
110	108	123	118	122	110	131	165	117	116
123	112	102	124	124	176	120	108	111	139
129	118	114	124	124	111	116	93	109	138
106	105	137	165	125	122	96	131	112	136
132	111	156	118	146	104	129	99	125	124
97	153	120	132	114	131	106	108	139	105
116	121	118	116	110	129	122	136	137	106
122	119	128	128	121	118	105	139	121	119

Table 3.1 100 TTFs simulated by the sample code in chapter 5, where N=100, VV=0.1, p=0.0001.

In our model, there are 3 main factors will affect the TTFs in a run: failure criteria, growth rate and nucleation rate. Failure criteria depends on how much percentage of phase transformation is defined as the time to failure. In this study, I would like to study these effects by building up a 2^3 design, which is shown in table 3.2. In each time of simulation, there are 10 TTFs generated by the Monte Carlo simulation, for Weibull distribution fit, shown in table 3.3 and figure 3.2. The design matrix is presented in table 3.4.

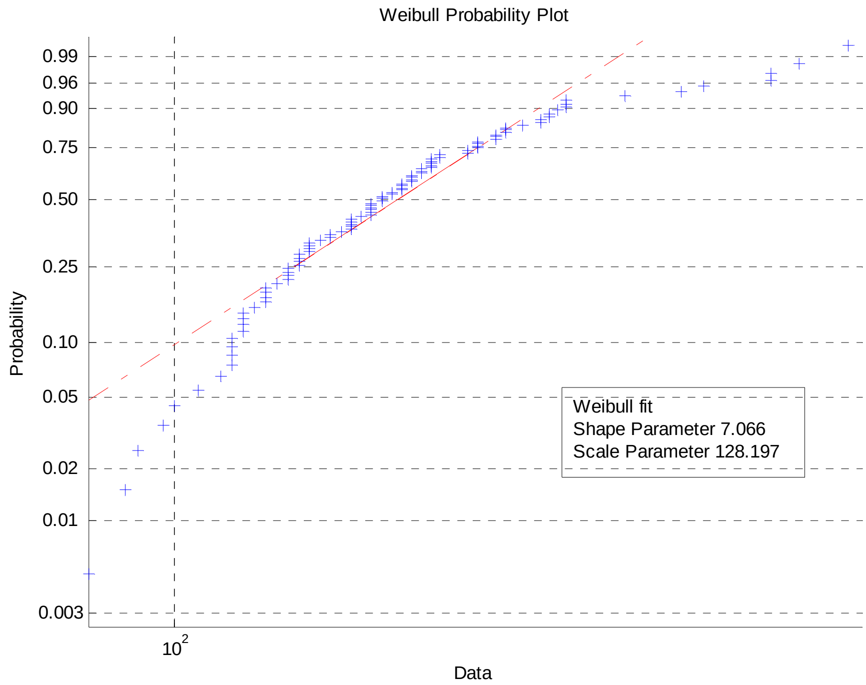

Figure 3.2 Weibull fit of 100 TTFs (in table 3.1) generated by the sample code in chapter 5, where N=100, VV=0.1, p=0.0001.

Factor	Level	
	-	+
A. Failure Criteria	80%	100%
B. Growth Rate	0.1	1
C. Nucleation Rate	0.0001	0.001

Table 3.2 Factors and Levels in the experimental data in table 3.3

run	Failure criteria	Growth rate (VV)	Nucleation rate (p)	TTFs	
1	80%	1	0.001	TTFs	11,11,12,12,12,11,13,12,13,12
				Log(TTFs)	2.4, 2.4, 2.5, 2.5, 2.5, 2.4, 2.6, 2.5, 2.6, 2.5
2	80%	0.1	0.001	TTFs	35,35,34,35,32,33,32,35,33,32
				Log(TTFs)	3.6, 3.6, 3.5, 3.6, 3.5, 3.5, 3.5, 3.6, 3.5, 3.5
3	80%	1	0.0001	TTFs	30,26,24,24,22,22,21,25,27,27
				Log(TTFs)	3.4, 3.3, 3.2, 3.2, 3.1, 3.1, 3.0, 3.2, 3.3, 3.3
4	80%	0.1	0.0001	TTFs	82,65,76,75,61,73,69,69,64,75
				Log(TTFs)	4.4, 4.2, 4.3, 4.3, 4.1, 4.3, 4.2, 4.2, 4.2, 4.3
5	100%	1	0.001	TTFs	20,24,18,20,22,19,19,19,24,22
				Log(TTFs)	3.0, 3.2, 2.9, 3.0, 3.1, 2.9, 2.9, 2.9, 3.2, 3.1
6	100%	0.1	0.001	TTFs	60,65,62,62,57,63,65,60,60,57
				Log(TTFs)	4.1, 4.2, 4.1, 4.1, 4.0, 4.1, 4.2, 4.1, 4.1, 4.0
7	100%	1	0.0001	TTFs	33,42,41,36,37,42,41,38,34,39
				Log(TTFs)	3.5, 3.7, 3.7, 3.6, 3.6, 3.7, 3.7, 3.6, 3.5, 3.7
8	100%	0.1	0.0001	TTFs	107,123,108,112,113,106,169, 100,115,119
				Log(TTFs)	4.7, 4.8, 4.7, 4.7, 4.7, 4.7, 5.1, 4.6, 4.7, 4.8

Table 3.3 Experimental data generated by Monte Carlo simulation

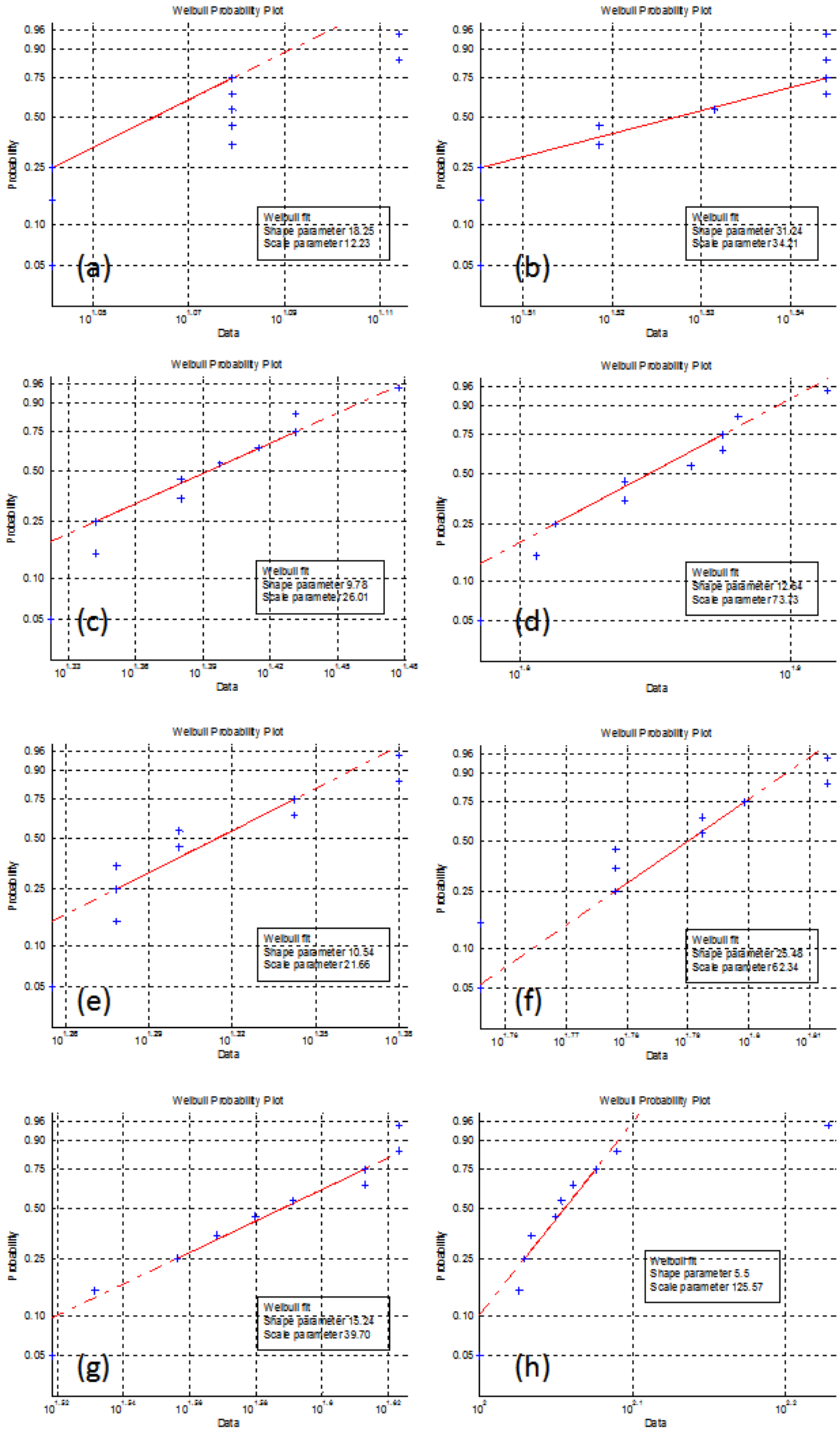

Figure 3.3 Weibull fit of the TTFs from (a) run 1, (b) run 2, (c) run 3, (d) run 4, (e) run 5, (f) run 6, (g) run 7, (h) run 8 shown in table 3.3

Factor A	B	C	Characteristic life time η from Weibull fit	Log(η)	Shape parameter β from Weibull fit	$\bar{y}$ (Log (TTFs))	s^2 (Log (TTFs))	$\ln s^2$ (Log (TTFs))
-	+	+	12.2342	2.504235	18.245	2.47	0.0038	-5.5638
-	-	+	34.211	3.532547	31.2406	3.51	0.0016	-6.4246
-	+	-	26.0143	3.258646	9.77591	3.21	0.0124	-4.3938
-	-	-	73.7251	4.300343	12.6422	4.26	0.0083	-4.7856
+	+	+	21.6628	3.075597	10.5418	3.03	0.0105	-4.5524
+	-	+	62.3846	4.133318	25.4828	4.11	0.0022	-6.1268
+	+	-	39.6955	3.681238	15.2386	3.64	0.0076	-4.8860
+	-	-	125.57	4.832863	5.50016	4.75	0.0211	-3.8607

Table 3.4 Design Matrix of the experimental data shown in table 3.3, where η and β are fitted by Weibull distribution

Since this work is deliberated to study the effects of factors (A, B, C) and their interactions on the two parameters (η and β) fitted by Weibull distribution, two Anova tables of three-way layout and factorial effects are shown in table 3.5 and table 3.6, respectively. The half-normal plots of the absolute effects on log(η) and β are presented in figure 3.4 and figure 3.5, respectively.

Source	Estimate	Sum of Squares	Degrees of freedom	Mean of Squares
A	0.532	0.56565	1	0.56565
B	-1.070	2.28911	1	2.28911
C	-0.707	0.99927	1	0.99927
AB	-0.035	0.00243	1	0.00243
AC	0.054	0.00589	1	0.00589
BC	0.027	0.00144	1	0.00144
ABC	0.020	0.00081	1	0.00081
Total		3.8646	7	

Table 3.5 Factorial Effects and Anova Table for Three-Way Layout of Log(η)

Source	Estimate	Sum of Squares	Degrees of freedom	Mean of Squares
A	-3.786	28.654	1	28.654
B	-5.266	55.464	1	55.464
C	10.588	224.226	1	224.226
AB	2.664	14.203	1	14.203
AC	-2.946	17.351	1	17.351
BC	-8.702	151.456	1	151.456
ABC	-3.638	26.463	1	26.463
Total		517.816	7	

Table 3.6 Factorial Effects and Anova Table for Three-Way Layout of shape parameter β

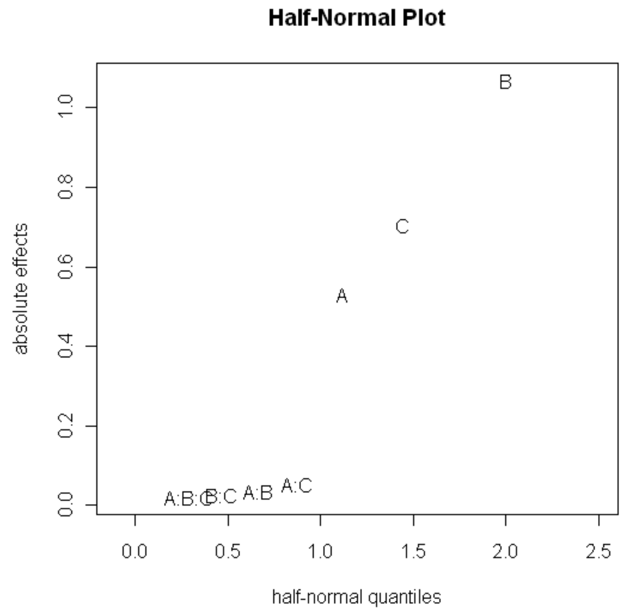

Figure 3.4 Half Normal Plot of Absolute effects on Log(η)

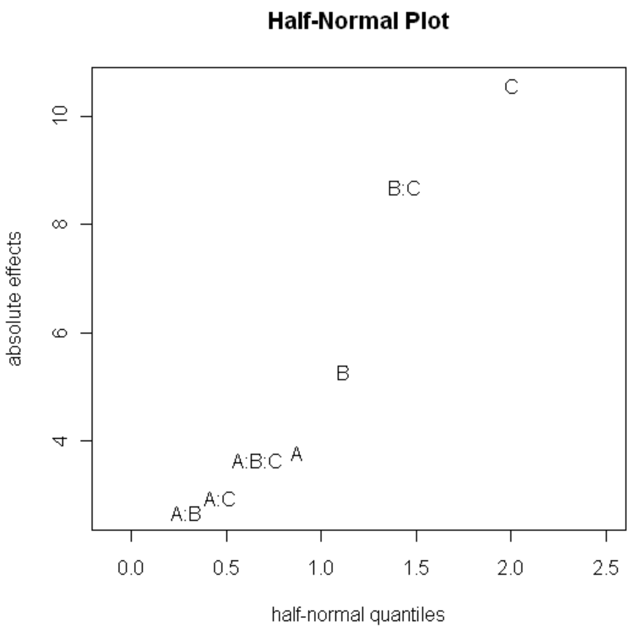

Figure 3.5 Half Normal Plot of Absolute effects on β

The half-normal plot shown in figure 3.4 indicates that the main factors A, B, C are more significant than the interaction factors on affecting log(η), thus η. In other words, the void growth rate (B) is the most significant effect on the characteristic time of Weibull distribution of the TTFs in the EM tests, followed by the void nucleation rate (C). Lower void growth rate (B-) and lower void nucleation rate(C-) result in longer characteristic time of the Weibull distribution of TTFs.

One the other hand, from the figure 3.5, it is found that the voids nucleation rate (C) is the most significant factor in affecting the shape parameter β, and the interactions between B and C also shows a significant effect on β in the second place. It is easy to find that a higher void nucleation rate (C+) can result in a higher β, representing that all the solder joints tested with such a failure mechanism will have a much less dispersed distribution of TTFs. Also, the interaction plot of B and C on affecting β, shown in figure 3.6, tells that low growth rate (B-) and high nucleation rate interaction (C+) is good for getting a higher β.

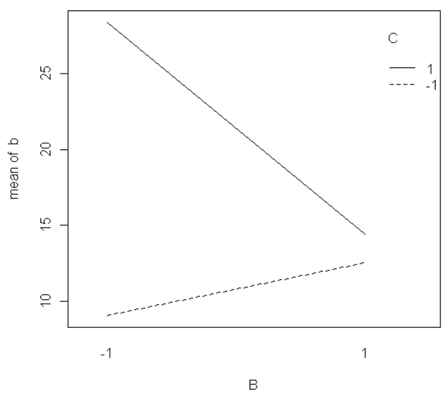

Figure 3.6 C-against-B Plots on affecting shape parameter β

The location effects and dispersion effects on Log(TTFs) are summarized in table 3.7, figure 3.7 and figure 3.8. The location effects of Log (TTFs) shows a same trend with the half-normal plot of absolute effects on Log(η). The dispersion effects plot of Log(TTFs) illustrates that the effect of nucleation rate (C) is the most significant factor, followed by B:C. Figure 3.9 shows the B and C interaction plot for the dispersion effects. It suggests that the choice of C(+) and B(-) will result in a less dispersion of Log (TTFs).

Effect	$\hat{y}$	$\ln s^2$
A	0.520	0.435475
B	-1.070	0.450425
C	-0.685	-1.185375
AB	-0.025	-0.175875
AC	0.060	0.219125
BC	0.010	0.767175

Table 3.7 Factorial Effects on Log(TTFs)

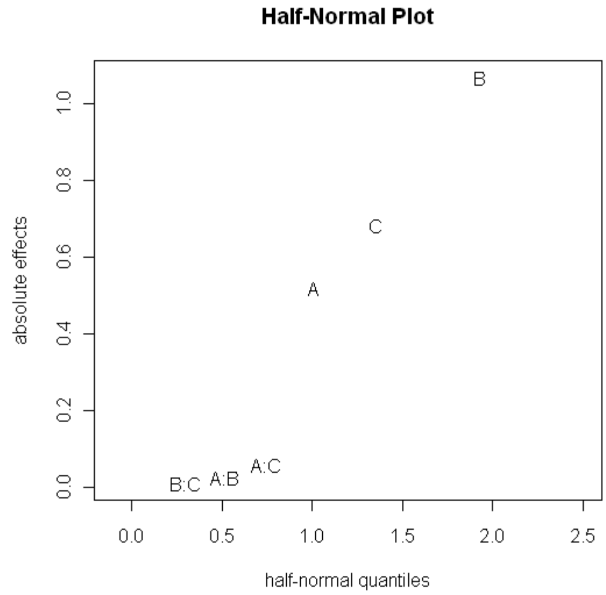

Figure 3.7 Location effects on Log(TTFs)

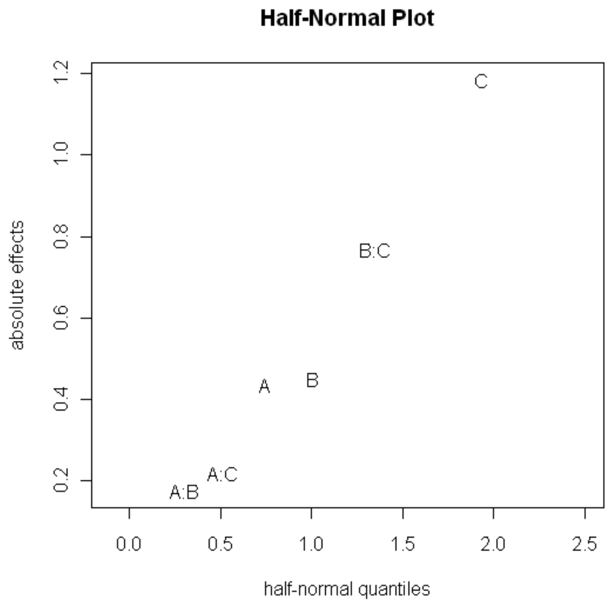

Figure 3.8 Dispersion effects on Log(TTFs)

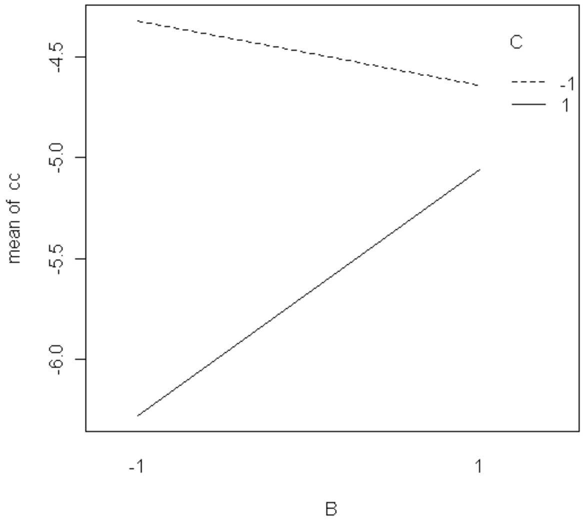

Figure 3.9 Interaction plot of B and C on dispersion effects on Log(TTFs)

To summarize the study in this work, a simplified model is built up for Monte Carlo simulation on the JMA phase transformation, which could describe the failure mechanism of flip chip solder joints in EM tests. A 2^3 experimental design is built to evaluate the effects of three main factors and their interactions: failure criteria, void nucleation rate and the void growth rate on the characteristic time η and the shape parameter β in Webull fit of TTFs.

From the statistical analysis, we can find that the void growth rate (B) affects the characteristic life time η more than others, followed by nucleation rate (C), indicating that in real cases, in order to get a longer TTF of the solder joints during EM tests, we would like to choose the materials which can slow down the void growth (B-) and void nucleation rate (C-) along the interface between solder and UBM. However, from the analysis in this work, to get a large shape parameter β (or minimize the dispersion of TTFs), which is favorable in real cases, the materials selection with a higher void nucleation rate(C+) and lower void growth rate (B-) during the EM tests will be helpful.

Indeed, the analysis results above just outline a conflict in materials selection between (B-C-) and (B-C+). However, in the most of real cases, the properties of a material, as the void nucleation rate and void growth rate, are not independent. Usually, a higher void nucleation rate is accompanied with a higher void growth rate. This could be the reason that it is relatively easier to get the flip chip solder joints to have a longer characteristic failure time by a proper materials selection, than to maximize the shape parameter of its TTFs Weibull distribution. To optimize the flip chip solder joints' TTFs distribution in EM tests, more effort is inevitable.

Chapter 4 Reference

1. http://en.wikipedia.org/wiki/Electronic_package
2. J. H. Lau, Chip on board technologies for multichip modules, Van Nostrand Reinhold, New York (1994)
3. http://en.wikipedia.org/wiki/Flip_chip
4. K. N. Tu, "Recent advances on electromigration in very-large-scale-integration of interconnects," J. Appl. Phys., 94, 5451-5473 (2003)
5. H. B. Huntington and A. R. Grone, "Current-induced marker motion in gold wires," J. Phys. Chem. Solids, 20, 76 (1961)
6. S. Gee, N. Kelkar, J. Huang, and K. N. Tu, ASME InterPACK Proceedings, IPACK 2005, p. 73417.
7. Black, J. R., "Electromigration - A Brief Survey and Some Recent Results". IEEE Transaction on Electron Devices (IEEE) ED-16 (4): 338.(1969).
8. M. Shatzkes and J. R. Lloyd, "A model for conductor failure considering diffusion concurrently with electromigration resulting in a current exponent of 2," J Appl. Phys, 59, 3890 (1986)
9. K. N. Tu, James W. Meyer, and Leonard C. Feldman, "Electronic thin film science for electrical engineers and materials scientists," Macmillan, NY (1992)."
10. http://en.wikipedia.org/wiki/Black%27s_equation
11. Melvin Avrami, Kinetics of phase change I—general theory, J. Chem. Phys. (7), 1103 (1939).
12. Melvin Avrami, Kinetics of phase change II—transformation-time relations for random distribution of nuclei, J. Chem. Phys. (8), 212 (1940).

13. Melvin Avrami, Granulation, phase change, and microstructure kinetics of phase change III, J. Chem. Phys. (9), 177 (1941).

14. Waloddi Weibull, “A statistical distribution function of wide applicability,” J. Appl. Mech.-Trans. ASME, 18 (3): 293–297 (1951).

15. J. W. McPherson, “Reliability physics and engineering: time-to-failure modeling.” Springer, Septermber (2010)

16. Lingyun Zhang, Shengquan Ou, Joanne Huang, K.N.Tu, Stephen Fee, and Luu Nguyen, "Effect of current crowding on void propagation at the interface between intermetallic compound and solder in flip chip solder joints", Appl. Phys. Lett. 88, 012106 (2006)

17. Yao Yao, Leon M. Keer, and Morris E. Fine, “Electromigration effect on pancake type void propagation near the interface of bulk solder and intermetallic compound”, Journal of Applied Physics, 105, 063710 (2009)

18. Ming-Hwa R. Jen, Lee-Cheng Liu, and Yi-Shao Lai, “Modeling of electromigration on void propagation at the interface between under bump metallization and intermetallic compound in flip-chip ball grid array solder joints”, Journal of Applied Physics 107, 093526 (2010)

19. Tian Tian, Kai Chen, A. A. MacDowell, Dula Parkinson, Yi-Shao Lai, and K. N. Tu, “Quantitative X-ray microtomography study of 3-C void growth induced by electronmigration in eutectic SnPb flip-chip solder joints”, Scripta Materialia 65, 646 (2011).

20. Tian Tian, Feng Xu, Jung Kyu Han, Daechul Choi, Yin Cheng, Lukas, Helfen, Marco Di Michiel, Tilo Baumbach and K. N. Tu, "Rapid diagnosis of

electromigration induced failure time of Pb-free flip chip solder joints by high resolution synchrotron radiation laminography", Applied Physics Letter 99, 082114 (2011)

21. J. H. Kinney, M. C. Nichols, "X-ray tomographic microscopy (XTM) using synchrotron radiation", Annu. Rev. Mater. Sci., 22 (1992), p. 121
22. L. Helfen, T. Baumbach, P. Mikulík, D. Kiel, P. Pernot, P. Cloetens and J. Baruchel, “High-resolution three-dimensional imaging of flat objects by synchrotron-radiation computed laminography”, Appl. Phys. Lett. 86, 071915 (2005).
23. L. Helfen, T. Baumbach, P. Cloetens, and J. Baruchel, “Phase-contrast and holographic computed laminography”, Appl. Phys. Lett. 94, 104103 (2009).

Chapter 5 Appendix

5.1 Sample code (run in MATLAB):

```
% velocity<1

format long;

vel=0.1;

 %velocity of the void void growth is 0.1 in this sample code

 rrow=0;ccol=0;row=0;col=0;

prob=zeros(100);

  % create a 100 × 100 matrix to storage the random number for selecting the new nucleation cells

  matA=zeros(100+2);

   % create a 100 × 100 matrix to storage the label the current phase of all cells

matB=zeros(100+2);

  % create a 100 × 100 matrix to storage the label the phase of all cells in last time step

matD=zeros(100+2);

  % create a 100 × 100 matrix to storage the change of all the cells in the last time step
```

```
prob=rand(100);
```

% generate a 100 × 100 matrix of random number indicating the nucleation probability of each cell

```
[row,col]=find(prob<0.0001);
```

% find all nucleation sites in the first time interval

```
len=length(row);
   for l=1:len
       matA(1+row(l),1+col(l))=10;
```

% nucleate new phase at the selected sites in the first time interval

```
   end
   t=1; % first time interval
   matD=matA;
   matB=matA;
while 100000-sum(sum(matA(2:101,2:101)))>0
```

% when 100% new phase formed, stop the run

```
        [rrow,ccol]=find(matD(2:101,2:101)==10);
```

% growth around new nucleation

```
llen=length(rrow);
   for ll=1:llen
      rr=rrow(ll)+1;
      cc=ccol(ll)+1;
      matA(rr-1:rr+1,cc-1:cc+1)=matA(rr-1:rr+1,cc-1:cc+1)+1
   end
rrow=0;ccol=0;

[rrow,ccol]=find(matD(2:101,2:101)>0 & matD(2:101,2:101)<10 &
matB(2:101,2:101)~=10);
% continue growth
llen=length(rrow);
   for ll=1:llen
      rr=rrow(ll)+1;
      cc=ccol(ll)+1;
      matA(rr,cc)=matA(rr,cc)+matD(rr,cc)
   end
```

```
rrow=0;ccol=0;

[rrow,ccol]=find(matD(2:101,2:101)>0 & matD(2:101,2:101)<10 &
matB(2:101,2:101)==10);
% growth around new cell just completes phase transformation by growth
llen=length(rrow);
  for ll=1:llen
    rr=rrow(ll)+1;
    cc=ccol(ll)+1;
    matA(rr-1:rr+1,cc-1:cc+1)=matA(rr-1:rr+1,cc-1:cc+1)+1
  end

prob=rand(100);
[row,col]=find(prob<0.0001);
% nucleation at the current time
len=length(row);
  for l=1:len
```

```
        matA(1+row(l),1+col(l))=10;
      end
    matA=min(matA,10)


    matD=matA-matB
    matB=matA
    t=t+1
    % write down the current time
    rrow=0;ccol=0;row=0;col=0;
end
```